

Bi-directional Graph Structure Information Model for Multi-Person Pose Estimation

Jing Wang¹, Junyi Sun¹, Ze Peng¹, Pei Lv^{1*}, Bing Zhou¹ and Mingliang Xu¹

¹ Zhengzhou University

* ielvpei@zzu.edu.cn

Abstract. In this paper, we propose a novel multi-stage network architecture with two branches in each stage to estimate multi-person poses in images. The first branch predicts the confidence maps of joints and uses a geometrical transform kernel to propagate information between neighboring joints at the confidence level. The second branch proposes a bi-directional graph structure information model (BGSIM) to encode rich contextual information and to infer the occlusion relationship among different joints. We dynamically determine the joint point with highest response of the confidence maps as base point of passing message in BGSIM. Based on the proposed network structure, we achieve an average precision of 62.9 on the COCO Keypoint Challenge dataset and 77.6 on the MPII (multi-person) dataset. Compared with other state-of-art methods, our method can achieve highly promising results on our selected multi-person dataset without extra training.

Keywords: Multi-person, confidence maps, geometrical transform kernel

1 Introduction

Human pose estimation is to estimate the locations of body joints from images and has become a fundamental research topic in many visual applications, such as action recognition [1,2,3], person re-identification [4], and human-computer interaction [5].

Significant advancements have been recently achieved in this field by convolutional neural networks (ConvNets). Some works [6,7,8,9] have used human detectors to obtain all the bounding boxes of individuals in an image and perform a single-person pose estimation in each of the detected bounding boxes. However, these top-down approaches do not work very well in complex or crowded environments where individuals cannot be detected accurately. Meanwhile, the other bottom-up [10,11,12,13] approaches directly predict all joints and assemble them into different individuals. Although much progress has been made in this research area, some challenging cases still exist, such as the wrong connections among joint points due to the unknown number of people, the ambiguous overlapping of joint points when the joint point of an individual is obscured by the

same joint point of another individual, and the keypoints that are occluded via self-occlusion or other-occlusion.

To address these problems, we propose a novel network architecture with two branches to estimate multi-person poses in images. The first branch predicts the confidence maps for each joint point and implements a geometrical transform kernel with a convolution layer to propagate information between neighboring joints at the confidence level. Compared with feature level, we can capture more explicit location information of the joints. The second branch proposes a new bi-directional graph structure information model (BGSIM), which, unlike [14], is a graph structure for multi-person pose estimation and incorporates the information transmitted among all joints to encode rich contextual information. BGSIM fully considers the occlusion relationship among different joints to solve self-occlusion or other-occlusion. Considering that one joint point with highest response of confidence maps contains most reliable information, we use it as the base point in BGSIM. The base point propagates information to other joints (especially for the occluded joints) via tree structures unrolled by our BGSIM, thereby ensuring reliable information that is transmitted among different body parts and facilitating the prediction of joint points.

With our proposed method, most of multi-person pose estimation cases can be solved directly. However, our proposed method may be unable to deal with situations wherein people get too close to each other, thereby producing almost coincident joint points in an image. In this case, we adopt the Integer Linear Programming (ILP) and the keypoint-based Non-Maximum-Suppression (NMS) mechanism that directly builds on the OKS metric (OKS-NMS) in the post-processing phase. The ILP labels and partitions the body part candidates, especially for the occluded keypoints, as well as facilitates the counting of people in an image, thereby avoiding false associations.



Fig. 1. Some image samples from our selected multi-person dataset. These images containing crowded people and high occlusion are chosen from the AI challenger, COCO, MPII, and LSP public datasets

Our proposed method achieves state-of-the-art results in the COCO and MPII benchmark datasets. We also construct a new dataset that contains 5899 images of multiple people with different degrees of occlusions. Some image samples are shown in Fig. 1. Our method outperforms other state-of-art methods on this new dataset.

The contributions of our work are summarized as follows:

- We design a novel network architecture with three stages to capture more explicit location information of body joints at the confidence level for multi-person pose estimation.
- We propose a BGSIM to encode rich contextual information and to infer occlusion relationship among different body parts.
- We determine the base point dynamically in BGSIM and use it as the root node for unrolled tree structures to propagate information to other joints.

2 Related Work

Automatic human pose estimation is crucial to intelligent surveillance systems, especially for human tracking and action recognition. Image-based human pose estimation in real-world environments remains a challenging task, and its current performance is still far from satisfactory due to occlusion and multi-person problems in complex scenes.

These problems are traditionally solved by using pictorial structures [15,16] or graphical models [17]. The Pictorial Structure Model [16] defines some pairwise connections of independent parts to represent the correlations among different body parts. However, the tree-structured model is “oversimplifie”. Accordingly, many researchers have proposed highly complex tree-structured models and the graph structure model [18]. Tian et al. [19] proposed a hierarchical spatial model that can capture an exponential number of poses with a compact mixture representation on each part. L. Pishchulin et al. [13] proposed a typical approach to articulate pose estimation by combining the spatial modeling of the human body with the appearance modeling of body parts. Meanwhile, other approaches [19,20,21,22,23,24,25,26,27] use the tree-structured or graphical model to solve the problems of human keypoints estimation and predict the keypoint locations based on handcrafted features (e.g., SIFT and HOG). With the rapid development of deep convolutional neural networks (CNN), recent studies [8,14,28,29,30,31,32,33,34,35] have made great process.

Single-Person Pose Estimation Early studies on human pose estimation have mainly focused on single-person pose estimation due to its simplicity. Toshev et al. introduced CNN to solve the pose estimation problem in Deep-Pose [28], which cascades CNN pose regressors to deal with the body joints. Wei et al. [34] and Newell et al. [36] found that deep CNNs perform effectively in human pose estimation as well as proposed a multi-stage architecture to solve the pose estimation problem. Newell et al. compiled several hourglass modules and proposed a U-shape architecture for human pose prediction. X. Chu et

al. [14] designed a structured feature-learning architecture to infer the correlations among different body parts at the feature level for human pose estimation. Although CNN can effectively extract feature information, the occlusion relationship among different body parts have not been fully explored.

Multi-Person Pose Estimation The above approaches show a promising performance in single-person pose estimation, but real-world images usually contain multiple persons. Multi-person pose estimation is a challenging task due to occlusion, the unpredictable interactions among different persons, and the diversity of human gestures. Some researchers have applied bottom-up approaches to deal with this problem. For instance, DeepCut [13] directly predicts all body part candidates, categorizes them into different classes, and partitions them into the corresponding people. DeeperCut [12] employs image-conditioned pairwise terms to achieve better pose estimation performance based on ResNet [37]. Cao et al. [10] mapped the relationship among different keypoints into part affinity fields (PAFs) and assembled the detected keypoints into different poses of people. In contrast to bottom-up approaches, top-down approaches initially locate each person and then independently analyze their joints. For example, Mask-RCNN [8] initially predicts the human bounding boxes and then crops out the feature map of these bounding boxes to predict the human keypoints. Papan-dreou et al. [6] predicted both the dense heatmaps and offsets of each keypoint type from each bounding box by using a fully convolutional resnet and then fused these heatmaps with offsets to obtain the final predicted location of keypoints. RMPE [9] predicts human pose by using the stacked hourglass model and then adjusted the imperfect proposal by combining STN, SPPE, and SDTN to overcome the location errors caused by the detection.

Nevertheless, these methods demonstrate a subpar performance in cases of multiple targets or serious occlusion. To address such limitations, we propose the BGSIM in our network architecture that can fully explore the connections among different body parts.

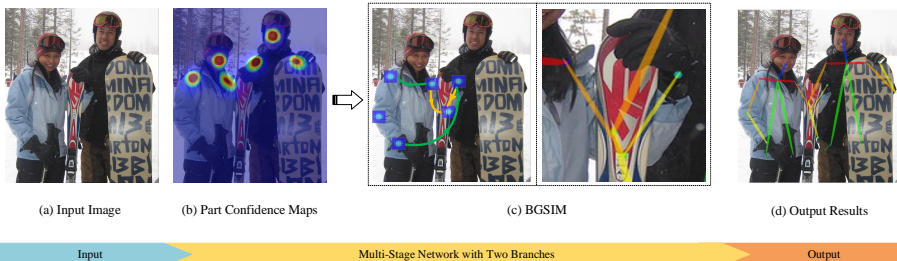


Fig. 2. Overall pipeline. Our method takes the entire image as the input for a multi-stage CNN network to predict the confidence maps for body part detection (shown in (b)) and for BGSIM (shown in (c)). The correct poses are eventually obtained for all persons in an image (shown in (d))

3 Our Method

Fig. 2 illustrates the overall pipeline of our method. A color image (Fig.2(a)) is taken as an input and the accurate locations of keypoints for each person in the image is eventually obtained (Fig.2(d)). First, a convolutional network predicts the confidence maps $c(x) = p(x|\sigma)$ of body part locations (Fig.2(b)) as defined in [38], where $x \in R^2$ denotes the joint location and σ denotes the types of joints. Second, BGSIM encodes rich contextual information, infers the occlusion relationship among different body parts, and transforms the underlying information from the visible joint points to the occluded ones (Fig.2(c)), thereby ensuring the true association.

3.1 Detection and Association

The network architecture of our method (shown in Fig. 3) predicts the confidence maps of detection and the occlusion information. The network has three stages, with each stage divided into two branches. The bottom branch predicts the confidence maps of joints, while the top branch predicts the occlusion information among different body parts. Each branch is an iterative prediction architecture.

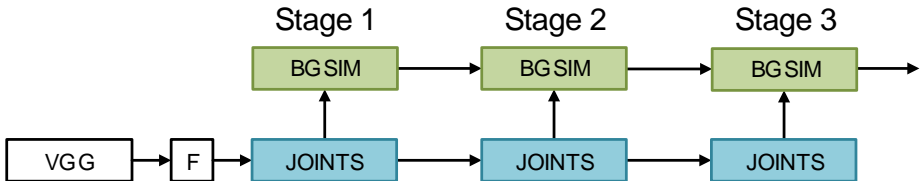


Fig. 3. The architecture of the three-stage CNN. Each stage has two branches, where the bottom branch, JOINTS, predicts the confidence maps of body joints, while the top branch, BGSIM, transmits the information among these body joints

The input image is analyzed by a convolutional network that is initialized with the first 10 layers of VGG-19 [39] and finetuned by changing the parameters of the last layer (the names, number of output, and coefficient of learning rate). This convolutional network generates the basic feature information $F=g(I)$ as input for JOINTS in the first stage, where I denotes the input image and g is a nonlinear function. At first stage, the JOINTS predicts the confidence maps of joint points as proposed in Section 3.2 and implements a geometrical transform kernel with a convolution layer to facilitate the information propagation between the confidence maps of neighboring body joints. For the heads and shoulders which are the stable human body parts, the JOINTS in first stage with less convolutional layers can predict the confidence maps of them. And the BGSIM as proposed in Section 3.3 in first stage only considers the confidence maps of heads and shoulders. At each stage, we use predictions of the JOINTS and previous

BGSIM as the input of this BGSIM. The elbows and hips with less flexible are predicted in the second stage. The third stage will consider all body joints. In some cases, the heads and shoulders are occluded and cannot be detected at stage 1. However, the other joints can still be detected and the other stages are still working. Nevertheless, the accuracy of human pose estimation may be affected by the loss of information about heads and shoulders.

3.2 Confidence Maps for Body Part Detection

As mentioned above, we need a reliable body part detection model to detect confidence maps of all the joints of a person before analyzing his or her pose. We use a deep, fully-convolutional human body part detection model that draws on powerful ideas regarding semantic segmentation, object classification, and human pose estimation.

We use a convolutional network that is initialized with the first 10 layers of VGG-19 [39] and finetuned by changing the parameters of the last layer. When obtaining the confidence maps, the geometrical transform kernels are used to propagate information between confidence maps similar to [14]. Compared with feature level, we can capture more explicit location information of the joints at the confidence level. For instance, the confidence maps of an input image for elbows and wrists are obtained by the convolutional network. If the elbow is occluded by other objects, then we cannot obtain its confidence map. In this case, we can shift the confidence map of the wrist toward the elbow by using geometrical transform kernel to solve the occlusion problem as shown in Fig. 4.

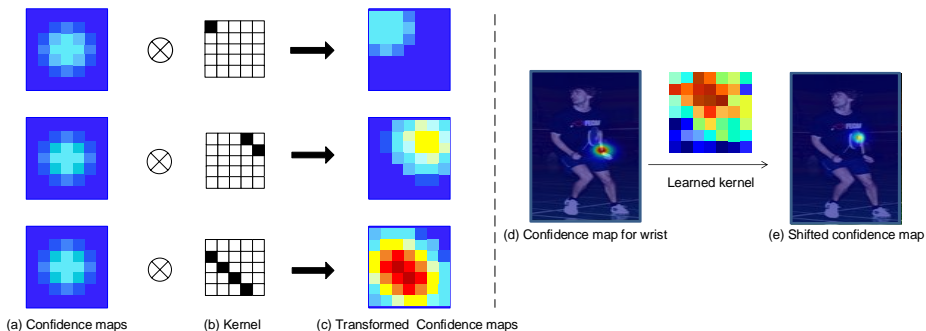


Fig. 4. (a)-(c) show that the confidence maps can be shifted through convolution with kernel, while (d)-(e) show an example of confidence maps that are shifted by learned kernel between adjacent joints

We obtain all confidence maps of each body part, but we are still uncertain whether these body parts belong to the same person. If we perform a regression among all body parts, then the regression result will be incorrect due to different shooting angles and occlusion. Compared with the traditional regression

architecture, CNN is robust to shooting angles and occlusion similar to [40]. We constrain the relationship among different body parts according to the BGSIM proposed in Section 3.3 to achieve highly accurate location results, and BGSIM is proven to be highly robust to shooting angles and occlusion.

3.3 BGSIM

Given that the tree-structured model is simple and cannot solve occlusion problem, we propose BGSIM based on graph-structured model. At each stage, our proposed BGSIM selects the joint with the highest response of confidence maps as the base point in this stage. (the orange joint point in Fig. 5) at each stage. Then we use the base point as the root node of a series of tree structures unrolled by our BGSIM to propagate information to other joints, especially for the occluded joints.

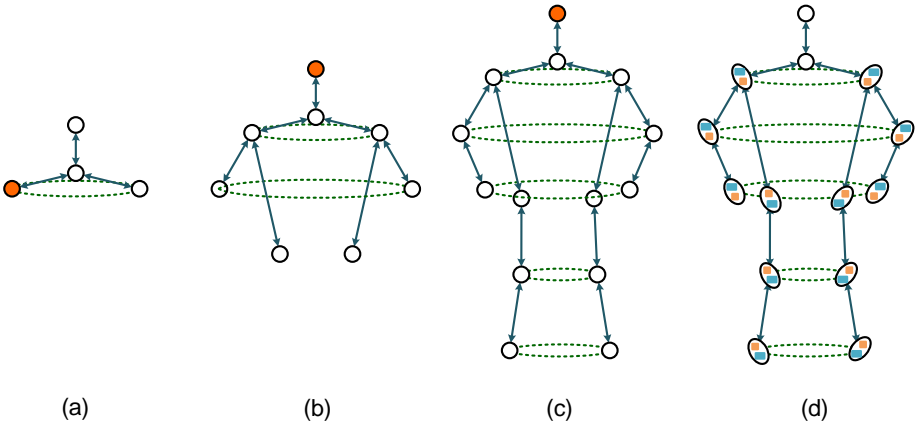


Fig. 5. The BGSIM at each stage and the unrolling of the model. (a) shows the BGSIM at the first stage, (b) and (c) show the BGSIM at the second and third stages, and (d) shows unrolling of the model

In the BGSIM, we denote $G = (V, \varepsilon)$ be the N -node graph, where V denotes the set of body parts, ε denotes the set of constraint edges and $N = |V|$ is the number of joint points. The position of the i joint point is denoted as $p_i = \{x_i, y_i\}$. The set of pairwise spatial relationships are denoted as $t = \{t_{ij}, t_{ji} | (i, j) \in \varepsilon\}$, where $t_{ij}, t_{ji} \in \{1, \dots, T_{ij}\}$ denotes the relative position between joint point i and j . $\phi = (p, t, o)$ is the pose configuration, $p = \{p_i\}$ and $o = \{o_i\}$, $o_i \in \{0, 1, 2\}$ is the occlusion state (“0” for visibility, “1” for self-occlusion, and “2” for occlusion by other objects).

Given an input image I , the goal of the BGSIM is to maximize the posterior as follows

$$P(\phi|I) \propto \left(\sum_{i \in V} U(I, p_i, o_i) + \sum_{(i,j) \in \varepsilon_K} R^K(t_{ij}, t_{ji}, o_i, o_j) + \sum_{(m,n) \in \varepsilon_C} R^C(t_{mn}, t_{nm}, o_m, o_n) \right) \quad (1)$$

where ε_K denotes the kinematic constraints among body parts, ε_C denotes the set of additional constraints among body parts that are not physically connected, and $\varepsilon = \varepsilon_K \cup \varepsilon_C$ denotes the full set of constraints. For simplicity, we call them to be kinetic edges (ε_K) and contextual edges (ε_C) respectively. In addition, $U(I, p_i, o_i)$ is the local part appearance score considering the occlusion state, while $R^K(t_{ij}, t_{ji}, o_i, o_j)$ and $R^C(t_{mn}, t_{nm}, o_m, o_n)$ represent the deformation (kinetic and contextual respectively) scores with occlusion coherence. The score function of BGSIM is formulated as:

$$S = \frac{F(I, \phi)}{|F(I, \phi)|} + \frac{F'(I, \phi)}{|F'(I, \phi)|} \quad (2)$$

$F(I, \phi)$ denotes score function with forward information flow (we define that the forward direction is from the base point to the end joint point of human body and the backward direction is opposite), $F'(I, \phi)$ denotes score function with backward information flow. The calculation of $F(I, \phi)$ and $F'(I, \phi)$ is same, so we only analyze the $F(I, \phi)$

$$F(I, \phi) = \sum_{i \in V} U(I, p_i, o_i) + \sum_{(i,j) \in \varepsilon_K} R^K(t_{ij}, t_{ji}, o_i, o_j) + \sum_{(m,n) \in \varepsilon_C} R^C(t_{mn}, t_{nm}, o_m, o_n) \quad (3)$$

the three terms on the right hand side of Eq.(3) handle occlusion from different aspects. The first term considers occlusion ‘‘local’’, i.e., whether each local part is visible, other-occluded or self-occluded. The second term encourages the occlusion states among physically connected parts to be continuous, while the third term reflects the self-occlusion relationship between physically non-connected parts.

In fact, we unroll the BGSIM formed at each stage into a tree model to generate the pose hypothesis and then rescore the candidate pose configurations with BGSIM. Afterward, we introduce the inference of the proposed model in the forward information flow and the inference of the proposed model in the backward information flow follows the same operation.

1) Model Unrolling: for any part i with an out-degree (number of connections pointing to the other parts) of $\nu_i > 1$, we generate $\nu_i - 1$ virtual parts and unroll the contextual edges to form a computation tree similar to [41] as shown in Fig. 6(d). The unrolled tree model is used to generate pose configurations.

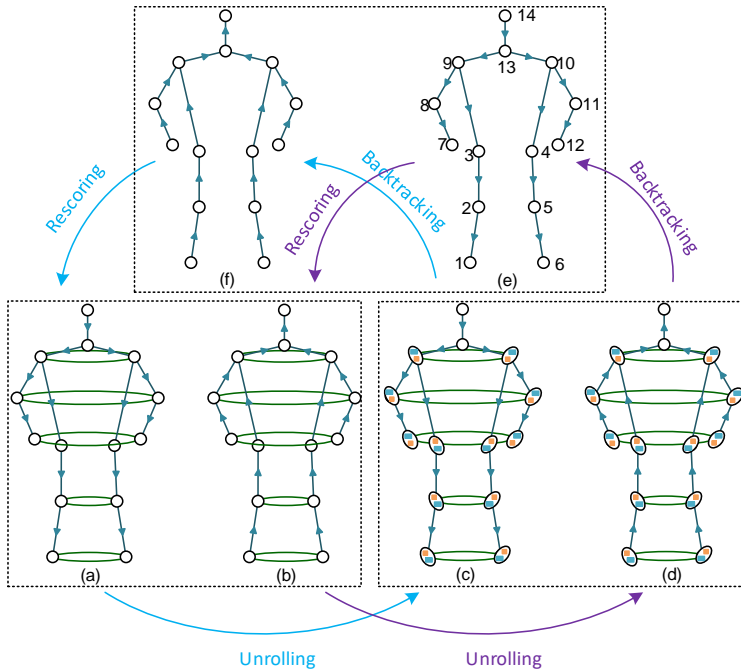


Fig. 6. Inference of BGSIM. (a) BGSIM in downward direction, (b) BGSIM in upward direction, (c) and (d) unrolled computation tree, and (e) and (f) nodes backtracked via the tree structure

2) Backtracking and Rescoring: The corresponding pose configurations can be obtained by backtracking directly from the root node to the leaf nodes. We only backtrack the child node from the real parent node (e.g., node 1 is backtracked from node 2 rather than node 6 in Fig. 6(e)) because the parent near the root node has less freedom of movement and is more reliable. We recompute the score of the pose configurations with a graphical model and rerank the hypothesis to obtain the optimal pose configuration.

3.4 ILP and OKS-NMS

Our network architecture can handle multi-person classification problems, but highly complex interlacing problems require further processing. Fig. 7(a) shows two people that almost coincide, while Fig. 7(b) shows an overlap among the same joints of different people. If we only use our network architecture to deal with these situations, then some misclassification or double detection of the same person will occur. Thus, we introduce ILP to address the joint points that are difficult to classify, and we use OKS-NMS to solve the overlapping joints.

We use ILP to label all candidates, place them in a body-part class (e.g., head, shoulder, and knee), and determine whether two different candidates belong to one person. Using the branch-and-cut algorithm [13] to compute the



Fig. 7. Some special cases. (a) presents a case where people almost coincide, (b) presents an overlap among the same joints of different people, and (c) shows detached overlapping joints in the scoremap by using OKS-NMS

constant-factor approximative feasible solutions of ILP is not necessarily practical. First, the time for computing the constant-factor approximative can increase along with the number of body part candidates in the worst case. Labeling and partitioning all body part candidates by using ILP will also consume much runtime. The runtime further increases along with the number of people in the input images. Second, considering all body part candidates for the entire image means that no distinction is made between the part classes that have been detected reliably (e.g., heads and shoulders) and the part classes that have been detected less reliably (e.g., wrists, elbows, and ankles). Therefore, we start with those body part classes that are detected most reliably before considering those body part classes that are detected less reliably. The body parts are divided into subsets {head, shoulder}, {elbow, hip}, and {wrist, knee, ankle}, thereby reducing the runtime effectively. For each subset, we obtain the density of confidence maps, and then use ILP when the density exceeds a certain threshold (0.5 in this paper).

Unlike traditional NMS, OKS-NMS in [6] does not completely remove the non-maximum detection keypoint but instead decays its score, thereby allowing us to separate overlapping joints and effectively reduce false joint connections.

4 Experimental Results

Our model is only trained on the COCO 2014 dataset and evaluated on two public benchmarks for person pose estimation, namely, the (1) COCO 2014 dataset and the (2) MPII human multi-person dataset. These two datasets contain many real-world challenging scenes, such as crowding, occlusion, and contact. Our approach demonstrates the same performance and even outperforms the other state-of-the-art methods on the COCO and MPII datasets, and shows its best performance in our own multi-person “occlusion” dataset with different levels of occlusion.

In our method, the first stage predicts the heads and shoulders, the second stage predicts the elbows and hips, and the third stage predicts the wrists, knees,

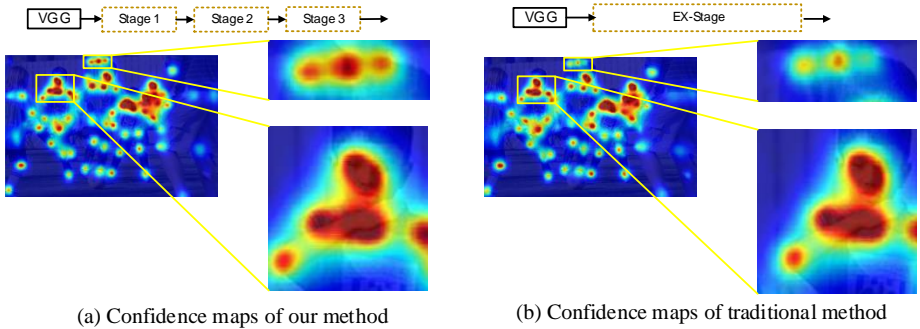


Fig. 8. The response of some occluded joints is strengthened by optimizing the three stages, and our method makes the response highly centralized and accurate

and ankles. Each stage shares the output information of the previous stage as the input to optimize the joints at this stage. Our method shows a very significant improvement in responding to some partially or severely occluded joints in a cascading way. Compared with traditional CNN architecture (Fig. 8(b)), the response of occluded joints in our architecture is strengthened by optimizing the three stages, and our method makes the response highly centralized and accurate. In our experiment, we use the convolutions with a kernel size of $7 * 7$. In fact, the larger kernel size has a larger receptive field, that can obtain rich global information, which is especially helpful when dealing with occluded joints.

4.1 Results on the COCO dataset

The training, validation, and testing sets of the COCO dataset contain over 200K images and 250K persons-instances-points labels with keypoints. Each person is annotated with 15 body joints for the full body. We apply the following object keypoint similarity (OKS) [42] defined by the COCO evaluation:

$$OKS = \frac{\sum_i \left[\exp\left(-\frac{d_i^2}{2s^2k_i^2}\right) \delta(v_i > 0) \right]}{\sum_i [\delta(v_i > 0)]} \quad (4)$$

The OKS is analogous to the IoU in object detection. By using OKS, we can compute the mean average precision (AP) and average recall (AR) as competing metrics. Table 1 shows the mAP of our method with different OKS thresholds and compares the mAP performance of our method with that of other approaches. For AP^{50} , our method outperforms the other methods and achieves an 85.1% AP. For AP^M , our architecture shows a slightly poorer performance than state-of-the-art architecture. Our architecture shows the best performance at AP^L and achieves 70.2% AP. Fig. 9 shows a breakdown of the errors of our method on the COCO validation set. Most of the false positives result from imprecise localization and background confusion, thereby indicating a large space

Table 1. Results on the COCO dataset. AP^{50} is the AP at OKS=0.5, and AP^L is the AP for a large-scale person

	AP	AP^{50}	AP^{75}	AP^M	AP^L
CMU-Pose	61.8	84.9	67.5	57.1	68.2
G-RMI	60.5	82.2	66.2	57.6	66.6
DL-61	54.4	75.3	50.9	58.3	54.3
R4D	51.4	75.0	55.9	47.4	56.7
umich_v1	46.0	74.6	48.4	38.8	55.6
Caltech	40.2	65.2	41.9	34.9	49.2
RMPE	61.8	83.7	69.8	58.6	67.6
Ours	62.9	85.1	69.7	56.7	70.2

for improvement in capturing spatial dependencies than in recognizing the appearance of body parts.

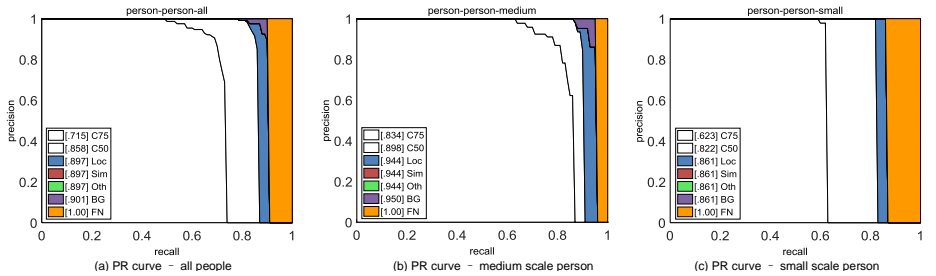


Fig. 9. AP performance on the COCO validation set in (a), (b), and (c)

4.2 Results on the MPII dataset

The MPII Human Pose dataset includes around 25000 images containing over 40000 persons with annotated body joints. We use the toolkit provided in [13] to measure the Average Precision (mAP) of all body parts based on the PCKh threshold. Table 2 compares the mAP performance of our method with that of other state-of-the-art methods. Compared with [10] and RMPE, our method shows the similar performance for some body parts, such as heads or shoulders. However, for other body parts that are easily occluded or show a large variation in the limb orientation (e.g., elbows or wrists), our method outperforms these two state-of-the-art methods. Unlike top-down methods such as RMPE, our method does not rely on human detection. Our method also shows the same performance as RMPE for single-person detection and can effectively detect multiple targets.

Table 2. Results on the MPII dataset

	Head	Shoulder	Elbow	Wrist	Hip	Knee	Ankle	Total
Iqbal&Gall, ECCV16 [43]	58.4	53.9	44.5	35.0	42.2	36.7	31.1	43.1
DeeperCut, EVVC16 [12]	78.4	72.5	60.2	51.0	57.2	52.0	45.4	59.5
Levinkov et al., CVPR17 [44]	89.8	85.2	71.8	59.6	71.1	63.0	53.5	70.6
Insafutdinov et al., CVPR17 [45]	88.8	87.0	75.9	64.9	74.2	68.8	60.5	74.3
Cao et al., CVPR17 [10]	91.2	87.6	77.7	66.8	75.4	68.9	61.7	75.6
RMPE [9]	88.4	86.5	78.6	70.4	74.4	73.0	68.5	76.7
Ours	90.7	87.7	80.2	71.1	74.8	72.9	66.3	77.6

Table 3. Results on our own dataset, where “+” indicates that we use ILP and OKS-NMS in the post-processing phase. When ILP is applied, the performance of the overall network increases by 4.5% AP to 43.6% AP

	AP	AP^{50}	AP^{75}	AP^M	AP^L	AR	AR^{50}	AR^{75}
CMU-Pose	39.7	57.3	41.9	36.2	42.6	40.6	49.1	41.2
Ours	39.1	57.6	40.6	37.5	41.6	41.3	48.8	42.2
Ours+	43.6	60.1	43.8	40.3	44.7	41.3	48.8	42.2

4.3 Results on our own dataset

Our dataset contains 5899 multi-person and high occlusion images that are selected from the AI challenger [46], COCO, MPII, and LSP public datasets. We directly evaluate the new dataset “occlusion” without any extra training. Table 3 compares our results on our own dataset with those of other methods. The performance of the network reaches 43.6% AP, which is 3.9% higher than that reported in [10]. Our method has a significant application value especially for pose estimation with high occlusions. Fig. 10 shows some experimental results on our own dataset. Given that the testing data in our own dataset are relatively dense and with high occlusion, we need to perform post-processing. We compare the results that are directly obtained by our method with those obtained by ILP and OKS-NMS (Ours+). As shown in Table 3, OKS-NMS can separate the two overlapping similar types of joints into two different joints, while ILP can cluster these joints to the right person. The proposed BGSIM+ outperforms the baseline BGSIM (43.6% AP vs. 39.1% AP) with only a minimal runtime loss.

5 Conclusion

In this paper, we follow the bottom-up pipeline for human pose estimation and propose a novel network architecture to address multi-person and occlusion problems in the estimation. Our network has two branches that predict the confidence maps of body joints and the occlusion relationship among these body joints. We also adopt ILP in the post-processing phase for those highly complex interlacing scenes with many people or almost coincident joint points. Our method achieves



Fig. 10. Experimental results on our own dataset, which images are selected from the AI challenger, COCO, MPII, and LSP public datasets

state-of-the-art results on the COCO keypoint and MPII benchmark datasets as well as achieves the best results on our own dataset without any extra training.

Our method can outperform the state-of-the-art methods under special cases with post processing. In our future work, we will refine the design of our proposed network architecture for different fields. For human pose estimation, we expect to develop a rational network architecture with a high accuracy, fast processing speed, and less computations even without post processing.

References

1. Wang, C., Wang, Y., Yuille, A.L.: An approach to pose-based action recognition. In: Computer Vision and Pattern Recognition. (2013) 915–922
2. Xu, R., Agarwal, P., Kumar, S., Krovi, V.N., Corso, J.J.: Combining skeletal pose with local motion for human activity recognition. In: Vii Conference on Articulated Motion and Deformable Objects. (2012) 114–123

3. Liang, Z., Wang, X., Huang, R., Lin, L.: An expressive deep model for human action parsing from a single image. In: IEEE International Conference on Multimedia and Expo. (2014) 1–6
4. Xiao, T., Li, H., Ouyang, W., Wang, X.: Learning deep feature representations with domain guided dropout for person re-identification. In: Computer Vision and Pattern Recognition. (2016) 1249–1258
5. Jain, H.P., Subramanian, A., Das, S., Mittal, A.: Real-time upper-body human pose estimation using a depth camera. In: International Conference on Computer Vision/computer Graphics Collaboration Techniques. (2011) 227–238
6. Papandreou, G., Zhu, T., Kanazawa, N., Toshev, A., Tompson, J., Bregler, C., Murphy, K.: Towards accurate multi-person pose estimation in the wild. (2017) 3711–3719
7. Huang, S., Gong, M., Tao, D.: A coarse-fine network for keypoint localization. In: IEEE International Conference on Computer Vision. (2017) 3047–3056
8. He, K., Gkioxari, G., Dollr, P., Girshick, R.: Mask r-cnn. (2017)
9. Fang, H.S., Xie, S., Tai, Y.W., Lu, C.: Rmpe: Regional multi-person pose estimation. (2016) 2353–2362
10. Cao, Z., Simon, T., Wei, S.E., Sheikh, Y.: Realtime multi-person 2d pose estimation using part affinity fields. (2016)
11. Newell, A., Huang, Z., Deng, J.: Associative embedding end-to-end learning for joint detection and grouping. (2016)
12. Insafutdinov, E., Pishchulin, L., Andres, B., Andriluka, M., Schiele, B.: Deepcut: A deeper, stronger, and faster multi-person pose estimation model. **42**(5) (2016) 34–50
13. Pishchulin, L., Insafutdinov, E., Tang, S., Andres, B., Andriluka, M., Gehler, P., Schiele, B.: Deepcut: Joint subset partition and labeling for multi person pose estimation. *Computer Science* **2008**(1) (2015) 4929–4937
14. Chu, X., Ouyang, W., Li, H., Wang, X.: Structured feature learning for pose estimation. In: IEEE Conference on Computer Vision and Pattern Recognition. (2016) 4715–4723
15. Fischler, M.A., Elschlager, R.A.: The representation and matching of pictorial structures. *IEEE Transactions on Computers* **C-22**(1) (1973) 67–92
16. Andriluka, M., Roth, S., Schiele, B.: Pictorial structures revisited: People detection and articulated pose estimation. In: Computer Vision and Pattern Recognition, 2009. CVPR 2009. IEEE Conference on. (2009) 1014–1021
17. Chen, X., Yuille, A.: Articulated pose estimation by a graphical model with image dependent pairwise relations. *Eprint Arxiv* (2014) 1736–1744
18. Fu, L., Zhang, J., Huang, K.: Orgm: Occlusion relational graphical model for human pose estimation. *IEEE Transactions on Image Processing* **26**(2) (2017) 927–941
19. Tian, Y., Zitnick, C.L., Narasimhan, S.G.: Exploring the spatial hierarchy of mixture models for human pose estimation. In: European Conference on Computer Vision. (2012) 256–269
20. Dantone, M., Gall, J., Leistner, C., Gool, L.V.: Human pose estimation using body parts dependent joint regressors. In: Computer Vision and Pattern Recognition. (2013) 3041–3048
21. Gkioxari, G., Arbelaez, P., Bourdev, L., Malik, J.: Articulated pose estimation using discriminative armlet classifiers. In: IEEE Conference on Computer Vision and Pattern Recognition. (2013) 3342–3349
22. Felzenszwalb, P.F., Huttenlocher, D.P.: Pictorial structures for object recognition. *International Journal of Computer Vision* **61**(1) (2005) 55–79

23. Sapp, B., Taskar, B.: Modec: Multimodal decomposable models for human pose estimation. In: *Computer Vision and Pattern Recognition*. (2013) 3674–3681
24. Wang, F., Li, Y.: Beyond physical connections: Tree models in human pose estimation. In: *Computer Vision and Pattern Recognition*. (2013) 596–603
25. Wang, Y., Duan, T., Liao, Z.: Learning hierarchical poselets for human parsing. In: *The IEEE Conference on Computer Vision and Pattern Recognition, CVPR 2011, Colorado Springs, Co, Usa, 20-25 June*. (2011) 1705–1712
26. Sapp, B., Jordan, C., Taskar, B.: Adaptive pose priors for pictorial structures. In: *Computer Vision and Pattern Recognition*. (2010) 422–429
27. Pishchulin, L., Andriluka, M., Gehler, P., Schiele, B.: Poselet conditioned pictorial structures. In: *Computer Vision and Pattern Recognition*. (2013) 588–595
28. Toshev, A., Szegedy, C.: Deeppose: Human pose estimation via deep neural networks. (2013) 1653–1660
29. Jain, A., Tompson, J., Lecun, Y., Bregler, C.: Modeep: A deep learning framework using motion features for human pose estimation. **9004** (2014) 302–315
30. Kang, K., Ouyang, W., Li, H., Wang, X.: Object detection from video tubelets with convolutional neural networks. In: *IEEE Conference on Computer Vision and Pattern Recognition*. (2016) 817–825
31. Ouyang, W., Zeng, X., Wang, X., Qiu, S., Luo, P., Tian, Y., Li, H., Yang, S., Wang, Z., Li, H.: Deepid-net: Deformable deep convolutional neural networks for object detection. *IEEE Transactions on Pattern Analysis Machine Intelligence* **PP**(99) (2016) 1–1
32. Bulat, A., Tzimiropoulos, G.: Human pose estimation via convolutional part heatmap regression. In: *European Conference on Computer Vision*. (2016) 717–732
33. Gkioxari, G., Toshev, A., Jaitly, N.: Chained predictions using convolutional neural networks. In: *European Conference on Computer Vision*. (2016) 728–743
34. Wei, S.E., Ramakrishna, V., Kanade, T., Sheikh, Y.: Convolutional pose machines. (2016) 4724–4732
35. Yang, W., Li, S., Ouyang, W., Li, H., Wang, X.: Learning feature pyramids for human pose estimation. (2017) 1290–1299
36. Newell, A., Yang, K., Deng, J.: Stacked hourglass networks for human pose estimation. (2016) 483–499
37. He, K., Zhang, X., Ren, S., Sun, J.: Deep residual learning for image recognition. In: *Computer Vision and Pattern Recognition*. (2016) 770–778
38. Zhang, K., Zhang, L., Yang, M.H., Zhang, D.: Fast tracking via spatio-temporal context learning. *Computer Science* (2013)
39. Simonyan, K., Zisserman, A.: Very deep convolutional networks for large-scale image recognition. *Computer Science* (2014)
40. Jain, A., Tompson, J., Andriluka, M., Taylor, G.W., Bregler, C.: Learning human pose estimation features with convolutional networks. *Computer Science* (2013)
41. Tatikonda, S.C., Jordan, M.I.: Loopy belief propagation and gibbs measures. In: *Eighteenth Conference on Uncertainty in Artificial Intelligence*. (2002) 493–500
42. : Mscoco keypoint evaluation metric. <http://mscoco.org/dataset/keypoints-eval>
43. Iqbal, U., Gall, J.: Multi-person pose estimation with local joint-to-person associations. (2016) 627–642
44. Levinkov, E., Andres, B., Uhrig, J., Tang, S., Omran, M., Insafutdinov, E., Kirillov, A., Rother, C., Brox, T., Schiele, B.: Joint graph decomposition and node labeling: Problem, algorithms, applications. (2016)
45. Insafutdinov, E., Andriluka, M., Pishchulin, L., Tang, S., Levinkov, E., Andres, B., Schiele, B.: Arttrack: Articulated multi-person tracking in the wild. (2016)

46. Wu, J., Zheng, H., Zhao, B., Li, Y., Yan, B., Liang, R., Wang, W., Zhou, S., Lin, G., Fu, Y.: Ai challenger: A large-scale dataset for going deeper in image understanding. (2017)